

MarineFormer: A Spatio-Temporal Attention Model for USV Navigation in Dynamic Marine Environments

Ehsan Kazemi¹ and Iman Soltani¹

Abstract—Navigating autonomously in marine environments including dynamic and static obstacles, and strong flow disturbances, such as in high-flow rivers, poses significant challenges for USVs. To address these challenges, we propose a novel methodology that leverages two types of attention: spatial attention, which learns to integrate diverse environmental factors and sensory information into navigation decisions, and temporal attention within a transformer framework to account for the dynamic, continuously changing nature of the environment. We devise MarineFormer, a Transformer-based navigation policy for dynamic Marine environments, trained end-to-end through reinforcement learning (RL). At its core, MarineFormer uses graph attention to capture spatial information and a transformer architecture to process temporal sequences in an environment that simulates a 2D turbulent marine condition involving multiple static and dynamic obstacles. We extensively evaluate the performance of the proposed method versus the state-of-the-art methods, as well as other classical planners. Our approach outperforms the state-of-the-art by nearly 20% in episode completion success rate and additionally enhances the USV’s path length efficiency. The project website is available at <https://soltanilara.github.io/MarineFormer/>.

I. INTRODUCTION

The main goal of the Unmanned Surface Vehicle (USV) studied here is to overcome environmental high current disturbances, avoid static and dynamic obstacles, and follow an optimal path toward a goal. Autonomous navigation in a dense environment, involving several static and dynamic obstacles, is a challenging problem even in the absence of external disturbances [1]. Under strong and spatially variable currents, the autonomous vessel and the surrounding dynamic agents are perturbed, further complicating the interactions.

Figure 1(a) visualizes the modeled marine environment studied in this research, where the direction and length of the black arrows correspond to the point-wise direction and magnitude of the current flow, respectively. The simulated currents are characterized by spatially varying distributions of eastward flows with random angles of attack, featuring singularities such as vortices, sinks, and sources. The vortices, sinks and sources effectuate circulating currents, strong attraction and repulsion, respectively. The static, and dynamic obstacles are represented as black and red circles, respectively. Since dynamic obstacles are constantly changing positions, they are only visualized in the supplementary videos and on the GitHub page of this article. The USV detects static obstacles via sensor I, a 2D proximity sensor

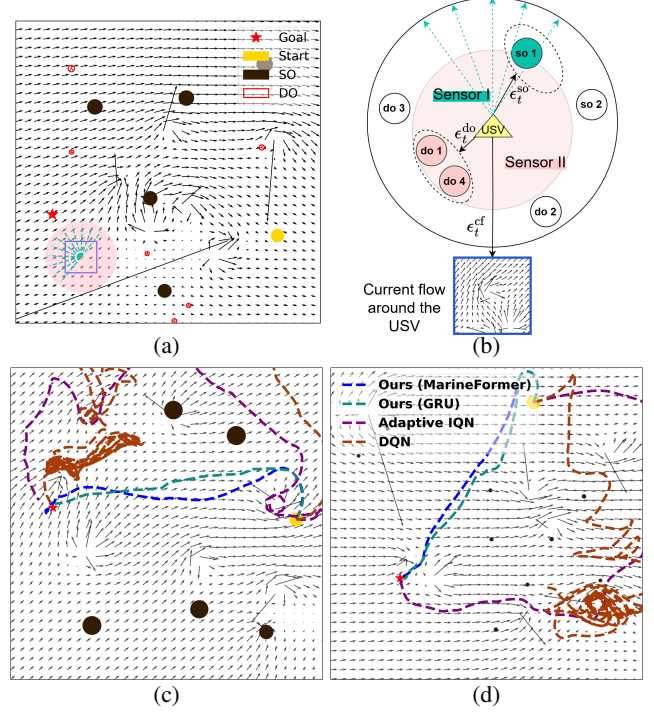


Fig. 1: (a) The simulated environment, including current flow, dynamic and static obstacles (do, so). (b) A graph model of the environment: edges indicate the attention of the USV to environmental components. (c, d) Example trajectories of our proposed method in comparison to baseline planners.

with a 180-degree front coverage (green dashed lines in Fig. 1(a)). Dynamic obstacles are detected by sensor II (the light red circle surrounding the agent) which has a 360-degree field of view. In addition to the obstacles, a flow sensor provides a rectangular map of the current velocity field in the vicinity of the USV (purple box). As shown in Fig. 1(b) the environment is modeled as a graph including multiple nodes namely the USV, dynamic obstacles (do), static obstacles (so), and the current flow (cf). The edges in this graph link the USV to observed environmental elements, representing its attention to them.

In this work, we use RL and leverage transformer architecture for path planning. Lately, the transformers [2] have significantly impacted the performance of Supervised Learning (SL) across a variety of tasks from computer vision to natural language processing, while demonstrating superior performance compared to traditional architectures. The common practice for treating temporal dependencies in RL is using recurrent neural networks (RNNs) [3]. Inspired by the

¹Laboratory for AI, Robotics and Automation, Department of Mechanical and Aerospace Engineering, University of California-Davis, CA 95616 USA (Corresponding author: Iman Soltani-isoltani@ucdavis.edu).

recent success of transformers in RL and also the deficiencies of RNNs to capture long-term temporal dependencies, this study focuses on further exploring the benefits of transformers to RL for autonomous navigation tasks. Given the multitude of sensory modalities often used in autonomous mobile systems, as well as the variety of environmental factors such as disturbances or obstacles, this work further explores the utility of spatial attention in trajectory planning.

The main contributions of this paper are as follows. 1) We propose a spatial attention mechanism to extract sensory information most relevant to navigation. 2) We propose a transformer-based policy network that captures dynamics of interaction between the robot, obstacles, and the environment with spatially variable flow disturbance hydrodynamics. 3) We propose a method to take into account the information about the flow dynamics surrounding the USV in learning a navigation policy and demonstrate that such information can significantly improve navigation performance. 4) A reward function is designed that enables the agent to mitigate the effect of flow disturbances while navigating through dynamic and static obstacles. 5) We provide a training recipe that enables effective end-to-end policy learning in a highly dynamic marine environment. 6) We compare the proposed policy against state-of-the-art RL-based approaches and conventional reaction-based methods. The results show that by using a properly designed reward function, the local flow measurements, and explicitly considering the future trajectory predictions of dynamic obstacles, as well as the likelihood of collision with static obstacles, the navigation safety of USVs in a dense environment is significantly improved. Our proposed approach improves episode completion success rate by 20% while enhancing the efficiency of planned trajectories compared to the state-of-the-art [4].

II. RELATED WORKS

The path-planning algorithms for USVs can be generally classified into pre-generative, reactive, and learning-based methods. Pre-generative approaches aim to find a safe path through known obstacles while satisfying path length or energy consumption constraints. Previously, researchers have developed diverse geometric-based algorithms such as the Fast Marching Method (FMM) [5]. Conventional reaction-based methods have been extensively used for robot navigation and obstacle avoidance. As a well-known example, Artificial Potential Fields (APF) [6] generate force fields to avoid obstacles and move towards the target but introduces challenges with local minima. Optimal Reciprocal Collision Avoidance (ORCA) [7] improved the performance of velocity collision avoidance approaches in multi-agent navigation problems by applying velocities following reciprocal obstacle avoidance behaviors. ORCA assumes availability of accurate velocity estimation and does not account for environmental disturbances. Learning-based methods tackle these limitations by learning the interactions in the environment and making decisions adaptively [8], [4].

Recently, the application of transformers in RL has seen rapid growth, yet it presents unique design challenges and

complexities inherent to RL's dynamic nature. In [9], a self-attention framework is leveraged for relational reasoning over state representations. However, in [10], it is shown that vanilla transformers are not suitable for processing temporal sequences, acting worse than a random policy for certain tasks. Gated Transformer-XL (GTrXL) [11] was introduced to enhance stability in RL by incorporating gating layers and Identity Map Reordering, which allowed for better gradient flow during training. In this work, we leverage transformers as temporal encoders. In a similar direction, [12] utilized temporal encoders for supervised tasks.

While obstacles are critical to consider in path planning and navigation control, in high-flow marine environments, the influence of environmental disturbances can be equally or even more significant, necessitating their inclusion for effective USV path planning. In [13], path planning with ocean currents is formulated as a multi-objective nonlinear optimization problem with overly flexible constraints. [14] introduced an anisotropic GPMP2 method that employs an energy consumption likelihood function for USV motion planning. Although effective in aligning with predefined current and obstacle patterns, this method fails to handle high obstacle densities or dynamic environments. [15] developed an improved RRT algorithm that applied motion constraints to shrink the sample space and accounted for ocean currents by adjusting the USV's velocity at each step. Although effective in utilizing time-varying ocean current predictions, this approach fails to adapt to highly dynamic environments with unpredictable changes. [16] derived time-optimal trajectories and strategies by defining and solving the level-set equation for the chasing problem in the presence of dynamic environmental disturbances. Although effective with predefined flow fields, this approach also fails to adapt to unpredictable environmental changes. In [17] comprehensive ocean information and physical constraints are taken into account to shorten time, improve speed, and conserve energy. This approach lacks flexibility in data-scarce environments requiring real-time adaptability.

Unlike previous work, our approach dynamically adapts to changing marine environments by leveraging spatio-temporal attention, offering greater flexibility and reliability in environments including high-density static and dynamic obstacles and unpredictable current conditions. Furthermore, our approach is grounded in practical constraints, limiting sensory measurements to current flow information from a local grid surrounding the vessel, and conventional sensors like sonar or LiDAR for obstacle detection.

III. METHODOLOGY

A. Approach

We tackle this problem using RL, formulated as a Markov Decision Process (MDP), defined by the tuple $\langle S, \mathcal{A}, \mathcal{P}, \mathcal{R}, \gamma, S_0 \rangle$, where S and \mathcal{A} are the sets of states and actions and S_0 is the set of initial states of the robot. $\mathcal{P}(s'|s, a)$ is the state transition function, with epistemic uncertainties rooted in the unknown nature of the environment e.g. caused by the unpredictability of the dynamic obstacles

as well as the surrounding flow, and aleatoric uncertainties due to noisy measurements. $\mathcal{R}(s, a)$ is the reward function and $\gamma \in [0, 1)$ is the discount factor. At each time step t , given the current state s_t , the agent chooses an action a_t , which leads to the transition $s_{t+1} \sim \mathcal{P}(\cdot | s_t, a_t)$ and the reward $r_t = \mathcal{R}(s_t, a_t)$. The goal of the agent is to maximize the expected return, $R_t = \mathbb{E}[\sum_{i=t}^T \gamma^{i-t} r_i]$, where γ is a discount factor. The value function $V^\pi(s)$ is defined as the expected return starting from the state s , and subsequently following policy π . The optimal policy π^* maximizes $V^\pi(s)$, which satisfies the Bellman optimality equation

$$V^{\pi^*}(s) = \mathbb{E}[r_t + \gamma \max_{s_{t+1}} V^{\pi^*}(s_{t+1}) | s_t = s]$$

where $s_{t+1} \sim \mathcal{P}(\cdot | s, a)$ and $a \sim \pi^*(s)$. The USV reaches a goal when its Euclidean distance to the goal is within the threshold d_{gt} during an episode of length T .

At each time step t , the policy receives information from the robot's ego-state, including its velocity and location, the states of static obstacles (so) and dynamic obstacles (do) within the robot's FOV, as well as the current flow (cf) conditions which is composed of pointwise measurements of velocity field within a rectangular grid surrounding the USV. The observation of states at time step t is expressed as $s_t = [s_t^{\text{ego}}, s_t^{\text{so}}, s_t^{\text{do}}, s_t^{\text{cf}}]$. $s_t^{\text{ego}} = [P_t^{\text{ego}}, V_t^{\text{ego}}]$ where $P_t^{\text{ego}} = [p_t^x, p_t^y]$, $V_t^{\text{ego}} = [v_t^x, v_t^y]$ are respectively the position and velocity of the USV at time t . s_t^{so} contains the position measurements collected from the static obstacles using a sensor such as sonar, $s_t^{\text{so}} = [O_t^{\text{so}_1}, \dots, O_t^{\text{so}_N}]$ where $O_t^{\text{so}_i}$ is the position measurement from the i^{th} beam of the sensor and N is the number of equally spaced radial beams emitted from the sensor I covering its FOV and range, M_R . If no obstacle is detected in the sensor range for the i^{th} beam, we set $O_t^{\text{so}_i}$ to twice the sensor range (i.e. $2M_R$). s_t^{do} contains the position and velocity of the moving obstacles within the FOV of sensor II featuring a similar range, M_R , as sensor I. It also includes the predicted future trajectory of each dynamic obstacle for a horizon of K time steps. $s_t^{\text{do}} = [O_t^{\text{do}_1}, \dots, O_t^{\text{do}_M}]$ where M is the number of dynamic obstacles in the environment, and $O_t^{\text{do}_j}$ is the concatenation of the current position and velocity of the j^{th} dynamic obstacle and the belief of the USV about its future trajectory, obtained from a trajectory prediction model. We have,

$$O_t^{\text{do}_j} = [P_t^{\text{do}_j}, V_t^{\text{do}_j}, \hat{P}_{t+1:t+K}^{\text{do}_j}] \quad (1)$$

where $P_t^{\text{do}_j} = [p_t^{\text{do}_j, x}, p_t^{\text{do}_j, y}]$, $V_t^{\text{do}_j} = [v_t^{\text{do}_j, x}, v_t^{\text{do}_j, y}]$ are the position and velocity of the j^{th} dynamic obstacle at time step t , and $\hat{P}_{t+1:t+K}^{\text{do}_j} = [\hat{p}_{t+1:t+K}^{\text{do}_j, x}, \hat{p}_{t+1:t+K}^{\text{do}_j, y}]$ the predicted future trajectory of the j^{th} dynamic obstacle over the horizon $t+1$ to $t+K$. It was shown previously [8] that incorporating information about the future states of moving obstacles can enhance the performance of learning-based methods for obstacle avoidance. Here, the trajectory prediction is obtained by assuming a constant velocity vector for the dynamic obstacles. If available, one can use the ground-truth future trajectories of the agents. As we use a fixed-size input for the dynamic obstacles, a binary mask is applied to filter out the

state of the undetected dynamic obstacles, e.g. those outside the sensor's FOV.

We further provide the policy with s_t^{cf} , a measurement of the flow velocity field on an $m \times m$ grid in the USV's ego-coordinate system within a rectangular area surrounding the USV (purple box in Fig. 1 (a)), i.e., $s_t^{\text{cf}} = \{V_{t,i,j}^{\text{cf}} = (v_{t,i,j}^{\text{cf},x}, v_{t,i,j}^{\text{cf},y})\}_{i,j=0}^m$, where i, j indicate the grid indices.

In real-world, the current flow field can be obtained in various ways, including Doppler sensors, vision cameras [18] or at a larger scale using satellite imagery. Utilizing local observations of the current flow enables the agent to reason about disturbances, and either avoid high-current regions of vortices, sources, or sinks or harvest flow energy if along the desired directions towards the goal.

B. Network Architecture

Our proposed architecture is composed of spatial and temporal attention mechanisms. The spatial component is based on a graph interpretation of the environment and is concerned with USV's attention to various aspects of the sensory measurements from flow or other obstacles in the environment which then feeds into a transformer, containing the temporal attention component and responsible for capturing the dynamics of the graph evolution over time. We begin by discussing the spatial-attention component of our proposed architecture, as illustrated in Fig. 2.

1) *Spatial attention to environment*: At each time step t , the spatio-temporal graph $G_t = (N_t^A, \epsilon_t^{A'})$ consists of a set of nodes N_t^A , where A can be USV, cf, do, and so, and a set of edges $\epsilon_t^{A'}$, representing the USV's attention to the environmental element A' , denoting the remaining nodes except the USV itself. The nodes, N_t^A , for USV, cf, so and do are defined respectively as s_t^{ego} , s_t^{cf} , s_t^{so} and \tilde{s}_t^{do} . \tilde{s}_t^{do} is an augmented version of s_t^{do} which is discussed later.

The spatial attention to A' at time t is computed using a query $Q_t^{A'}$ and key $K_t^{A'}$, and applies the resulting score to a value vector $V_t^{\text{attn}, A'}$. The attention edges are then given as:

$$\epsilon_t^{A'} = \text{softmax} \left(\frac{Q_t^{A'} K_t^{A'^T}}{\sqrt{d}} \right) V_t^{\text{attn}, A'} \quad (2)$$

where d is the dimension of the query and key. For ϵ_t^{cf} , the query Q_t^{cf} is generated as an embedding of s_t^{ego} . For ϵ_t^{do} and ϵ_t^{so} , the queries, Q_t^{do} , and Q_t^{so} are generated as embeddings of ϵ_t^{cf} , enabling direct consideration of flow disturbances when attending to obstacles. The key $K_t^{A'}$ and value $V_t^{\text{attn}, A'}$ for $A' = \text{'cf'}$, 'do' and 'so' are embeddings of their corresponding nodes i.e. N_t^{cf} , N_t^{do} and N_t^{so} , respectively.

We give special attention to the dynamic obstacles, as they form one challenging aspect of the given navigation task. For this purpose, the state of dynamic obstacles (Eq. 1) are augmented to incorporate their mutual alignment. By incorporating this information, the proposed model can capture a holistic view of obstacle movement patterns and identify preliminary estimates of potential collision zones, such as areas where multiple obstacles may converge or where closing gaps might block future paths. For M dynamic

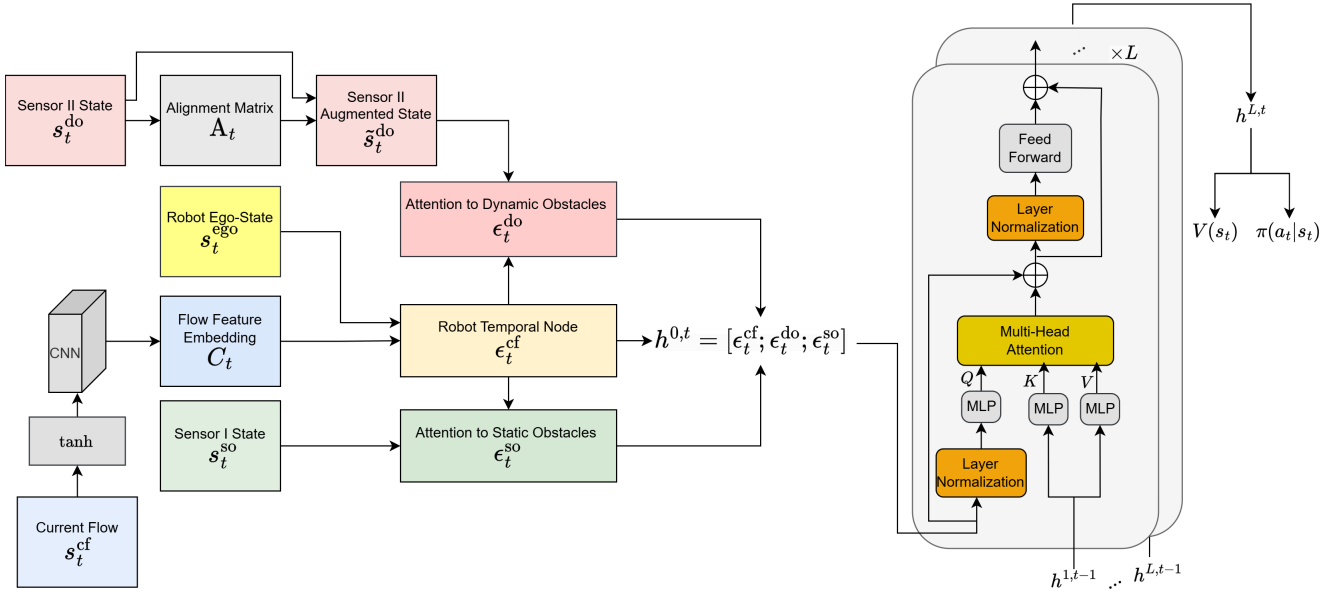


Fig. 2: The architecture of our proposed MarineFormer model.

obstacles in the FOV of the USV, we define an M by M alignment matrix, \mathbf{A}_t , given as:

$$\mathbf{A}_t = \text{softmax}(\mathbf{B}_t \mathbf{D} \mathbf{D}^T \mathbf{B}_t^T) \quad (3)$$

where softmax operates column-wise, \mathbf{D} is a trainable diagonal weight matrix and \mathbf{B}_t is a matrix containing the states of the dynamic obstacles, i.e.

$$\mathbf{B}_t = \begin{bmatrix} O_t^{\text{do}_1} \\ \vdots \\ O_t^{\text{do}_M} \end{bmatrix} \quad (4)$$

The state of the j^{th} dynamic obstacle in Eq. 1 is then concatenated with the corresponding alignment vector on the j^{th} row of the alignment matrix to obtain the augmented state $\tilde{O}_t^{\text{do}_j}$, i.e.,

$$\tilde{O}_t^{\text{do}_j} = [O_t^{\text{do}_j}, \mathbf{A}_t^j] \quad (5)$$

where \mathbf{A}_t^j is the j^{th} row of \mathbf{A}_t . The state of the dynamic obstacles and hence, the corresponding node, N_t^{do} , is updated as $N_t^{\text{do}} = \tilde{s}_t^{\text{do}} = [\tilde{O}_t^{\text{do}_1}, \dots, \tilde{O}_t^{\text{do}_M}]$.

All Q , K , and V embeddings associated with attention to various nodes, except ϵ_t^{cf} , are obtained by learning the parameters of their corresponding multilayer perceptrons (MLPs). For ϵ_t^{cf} , the current flow node, $N_t^{\text{cf}} = s_t^{\text{cf}}$, is first transformed to the USV coordinate and mapped to the interval $[-1, 1]$ using tanh. It is then processed through a convolutional layer which processes the channels associated with x and y components of the velocity separately to obtain a latent representation denoted C_t . K_t^{cf} and $V_t^{\text{attn,cf}}$ are derived by passing C_t through MLPs. This aspect of the architecture enables the policy to learn and attend to the relevant spatial features of the flow map, such as strong velocity gradient

patterns indicative of flow singularities (e.g., vortices, sinks, and sources characterized by the $1/r$ multiplier), as well as the overall pull direction and disturbance intensity, thereby supporting robust trajectory planning.

2) *Capturing Temporal Dependencies through Transformer*: The graph G_t evolves over time due to the movement of agents, and location dependence of the external flow disturbances. To capture the dynamics of the environment, we rely on a transformer module (Fig. 2). The input to the first layer of the transformer, $h_{0,t}$, is composed of all the graph attention edges, $\epsilon_t^{A'}$ i.e. $h_{0,t} = [\epsilon_t^{\text{cf}}, \epsilon_t^{\text{do}}, \epsilon_t^{\text{so}}]$. The transformer output $h_{L,t}$ at the L^{th} layer is fed to a fully connected layer to obtain the value $V^\pi(s_t)$ and the policy $\pi(a_t|s_t)$. As indicated in Fig. 2, the transformer is composed of a stack of L identical layers. Each layer has two sub-layers. The first is a multi-head cross-attention between $h_{l-1,t}$ and the output of l^{th} layer from the previous time step $h_{l,t-1}$ and the second is a fully connected layer. We employ a residual connection for each of the two sub-layers, preceded by layer normalization. All the L layers produce outputs of the same dimension.

C. Reward Function

The reward function is defined as follows

$$r_t = \mathbf{1}_{\text{collision}}(s_t) r_c + \mathbf{1}_{\text{goal}}(s_t) r_g + \mathbf{1}_{\text{collision}^c \cap \text{goal}^c}(s_t) (r_t^{\text{pot}} + r_t^{\text{do}} + r_t^{\text{so}} + r_t^{\text{cf}}) \quad (6)$$

$\mathbf{1}_{\text{collision}}$ and $\mathbf{1}_{\text{goal}}$ are the indicator functions activated when the state s_t corresponds to a collision or arrival at the goal, respectively. The penalty (negative value) for collision and the reward for arriving at the goal are denoted as r_c and r_g , respectively. The indicator function $\mathbf{1}_{\text{collision}^c \cap \text{goal}^c}$ is active for states s_t that are in neither the collision state nor the goal state. $r_t^{\text{pot}} = \alpha (dist_{t-1}^{\text{goal}} - dist_t^{\text{goal}})$ is a potential-based reward to guide the USV towards the goal, in which $dist_t^{\text{goal}}$

is the L_2 distance to the goal at time t and α is a scalar hyperparameter. Due to the nonholonomic kinematics of the differential thrust assumed for the USV, which limits its maneuverability, proximity to obstacles poses a high risk of collision. To prevent such cases, we use the penalties r_t^{do} and r_t^{so} to discourage such intrusions:

$$\begin{aligned} r_t^{\text{do}} &= \min_{i=1,\dots,M} \min_{k=1,\dots,K_{\text{do}}} \left(\frac{\mathbf{1}_{\text{collision}}^i(\hat{s}_{t+k}) r_c}{2^{k+2}} \right) \\ r_t^{\text{so}} &= \min_{i=1,\dots,N} \min_{k=1,\dots,K_{\text{so}}} \left(\frac{\mathbf{1}_{\text{collision}}^i(\hat{s}_{t+k}) r_c}{2^{k+2}} \right) \end{aligned} \quad (7)$$

where M and N are the number of dynamic and static obstacles, respectively. $\mathbf{1}_{\text{collision}}^i$ is active when the USV collides with i^{th} obstacle at the predicted state \hat{s}_{t+k} . We assign a smaller penalty for intrusions projected to occur farther in the future. To compute r_t^{do} we use the predicted trajectories of both USV and the dynamic obstacles for potential collision, while r_t^{so} only uses the prediction of the USV trajectory. The collision prediction horizon for dynamic and static obstacles are K_{do} and K_{so} time steps, respectively. Per Eq. 7, the penalty value is driven by a single obstacle (minimum with respect to i) associated with the most imminent (minimum with respect to k) predicted collision.

The attraction force from sinks can lead to a stagnation state where thrusters are unable to generate enough force to escape. Similarly, when caught in strong flows, the agent may fail to approach the goal. To reward policies that avoid such scenarios, the r_t^{cf} component of Eq. 6 penalizes by r_{cf} those scenarios where the USV fails to move closer to the target by at least the distance \bar{d}_{cf} in a single time step, i.e.,

$$r_t^{\text{cf}} = \begin{cases} r_{\text{cf}} & \text{if } \text{dist}_{t-1}^{\text{goal}} - \text{dist}_t^{\text{goal}} < \bar{d}_{\text{cf}}, \\ 0 & \text{otherwise.} \end{cases} \quad (8)$$

IV. EXPERIMENTS

A. Experiment Settings

We consider two training scenarios as shown in Fig. 1; the first scenario (Fig. 1c) consists of 10 dynamic obstacles and 5 static obstacles. The second scenario (Fig. 1d) consists of 25 dynamic obstacles and 10 static obstacles. The radius of static obstacles in scenario I is randomly chosen from the range $[1.0, 1.5]m$, while in scenario II, the radius is randomly selected from the range $[0.2, 0.3]m$. In other words, the size of static obstacles for scenario I is on average 5 times larger than scenario II. All dynamic obstacles are controlled by ORCA and react to other dynamic obstacles, not the USV. This prevents the USV from learning a policy that leverages the yielding of the dynamic obstacle. The radius of dynamic agents is set to $0.3m$ with a maximum velocity of $2m/s$ and FOV of 2π rad. We assume that within an episode, the dynamic obstacles occasionally change their goals to other random positions and that the current flow does not impact the trajectory of dynamic obstacles. Our environment, accommodating all obstacles within a $40m \times 40m$, rectangle, is significantly denser than those in previous works [19], [4], presenting a more challenging obstacle avoidance problem.

In each episode, the start and the goal positions of the USV, the location of obstacles, the angle of attack for the uniform flow, and the distribution of flow singularities, i.e., centers of vortices, sinks, and sources, are randomly initialized. The uniform flow has a magnitude of $V^{\text{uniform}} = 1m/s$ with a random angle of attack chosen from the interval $[0, \pi/4]$ rad. The velocity field of the current flow is simulated using potential flow techniques with vortices, sinks and sources in addition to the uniform flow component [20]. For each environment, we generate 4 vortices, and 4 total sinks/sources. The intensity of a vortex is characterized by Γ , which fully defines the flow tangential velocity at distance r from the center, given by $V_{\theta}^{\text{vortex}} = \Gamma/(2\pi r)$. Similarly, sinks, and sources are characterized by Λ , determining their radial flow velocity at distance r , given by $V_r^{\text{sink/source}} = \Lambda/(2\pi r)$. For each singularity, Λ and Γ are randomly selected from the range $[5\pi, 10\pi]$. The centers of flow singularities are chosen such that the distance between any two singularity is greater than the sum of their corresponding radius. The radius of each singularity is a distance from the center where the flow field transitions back to the predefined uniform flow velocity (V^{uniform}). At any given position $p = [p^x, p^y]$, the total flow velocity field is obtained as a superposition of individual velocity components, i.e. $V_p^{\text{cf}} = V_p^{\text{source}} + V_p^{\text{sink}} + V_p^{\text{vortex}} + V^{\text{uniform}}$.

B. USV Dynamics

The first order dynamics model in [21] is used for the USV in the presence of current flow, given by:

$$\frac{dP_t^{\text{ego}}}{dt} = V_t^{\text{ego}} = V_{P_t^{\text{ego}}}^{\text{cf}} + V_t^{\text{steer}} \quad (9)$$

where as noted before V_t^{ego} is the USV velocity in the world coordinate, V_t^{steer} is its steering velocity and $V_{P_t^{\text{ego}}}^{\text{cf}}$ is the current flow velocity at the USV position P_t^{ego} . We assume differential thrust for the simulated USV. The USV action at time step t is $\mathbf{a}_t = (\Delta v_t, \Delta \theta_t)$, where Δv_t is the change in the steering speed (change in the magnitude of V_t^{steer}), and $\Delta \theta_t$ is the change in the heading of the USV. The navigation policy is described as $\pi : s_t \rightarrow (\Delta v_t, \Delta \theta_t)$. The action space is continuous and Δv_t and $\Delta \theta_t$ are capped, respectively to the ranges $[-0.1, 0.1]m/s$ and $[-0.1, 0.1]$ rad to reflect the specifications of the USV thrusters and also indirectly cap linear and rotary accelerations. We chose the control time step $\Delta t = 0.25s$. The actions are used to update the steering speed of the USV, through the following equations:

$$\begin{aligned} v_{t+1}^{\text{steer}} &= v_t^{\text{steer}} + \Delta v_t \\ \theta_{t+1}^{\text{steer}} &= \theta_t^{\text{steer}} + \Delta \theta_t \end{aligned}$$

, where $v_t^{\text{steer}} = \|V_t^{\text{steer}}\|$ and therefore the steering velocity vector V_{t+1}^{steer} is obtained as follows

$$V_{t+1}^{\text{steer}} = [v_{t+1}^{\text{steer}} \cos(\theta_{t+1}^{\text{steer}}), v_{t+1}^{\text{steer}} \sin(\theta_{t+1}^{\text{steer}})]$$

We assume that sensor I which is forward-looking to detect static obstacles, has 11 beams covering a π rad field of view, while sensor II, used to detect moving obstacles, has a

2π rad, field of view. Both sensors have a range of $5m$. In a practical implementation, sensors I and II may respectively represent a forward-looking sonar and a 360-degree LiDAR. It is noted that the number, nature, and FOV of the sensors may be updated to reflect the specifics of a given USV setup. We assume a constant velocity vector, based on the latest measurements, to predict the future trajectory of dynamic obstacles in Eq. 1 along a straight line. The current flow measurements are captured from an 8×8 rectangular grid of size $5m \times 5m$ surrounding the vessel.

We compare our approach with two reaction-based methods. We use ORCA as one baseline where the agents avoid each other under the reciprocal rule [22], [7]. As another classic local planning baseline, we choose APF method [6]. This approach constructs an attractive potential field U_{att} and a repulsive potential field U_{rep} to generate forces that guide the USV toward its goal while repelling it from obstacles. For a given observation, the repulsive force is the sum of contributions from all obstacles.

We further compare our model's performance to the learning-based approach for USV collision avoidance presented in [4]. Their work is based on implicit quantile networks (IQN) [23], which expresses the return distribution with a quantile function and enables the incorporation of a distortion risk measure to compute a risk-distorted expectation for the Q-function as well as a risk-sensitive policy. The RL model is trained using IQN loss which is constructed from quantile Huber loss. The control time step in this baseline is $\Delta t = 0.05$, and the linear acceleration a and angular velocity ω are selected from the discretized space $a \in \{-0.4, 0, 0.4\}m/s^2$, and $\omega \in \{-0.52, 0, 0.52\}rad/s$. As our control time step is 5 times larger, we selected comparable bounds for Δv_t and $\Delta \theta_t$ in our approach to ensure a fair comparison to this method. We also choose DQN [24] as a traditional DRL baseline, and use the implementation from [24]. As part of our ablations and to investigate the utility of the transformer module within our proposed MarineFormer architecture, we further consider a variation of our method in which the transformer is replaced with a GRU.

C. Evaluation

In this implementation of MarineFormer, the number of attention heads and transformer layers are both set to 1. For the reward function (6), we set $r_c = -20$, $r_{cf} = -0.2$ and $r_g = 10$. K_{do} and K_{so} in (7) are set to 5 and 3 respectively. We set \bar{d}_{cf} in Eq. (8) to 0.2.

In each step, the experience tuple (s, a, r, s') of the USV is inserted into the replay buffer \mathcal{M} . We use PPO, a model-free policy gradient algorithm for policy and value function learning [25]. In the PPO we set the coefficient of value loss to 0.5. We perform training in 32 processors (environments). We assume a minimum of $12m$ distance between the start point and the goal location, and a minimum of $5m$ separates the initial location of obstacles. The time limit of each episode is set to $110s$ which is equivalent to 440 steps. We use Adam optimizer with learning rate $4e-5$, $\beta_1 = 0.9$, $\beta_2 = 0.999$, and $\epsilon = 1e-5$ without weight decay,

Method	scenario I		scenario II	
	SR	PL	SR	PL
APF	62%	201.84	60%	195.23
ORCA	7%	112.46	5%	105.57
DQN	68%	106.98	69%	83.77
Adaptive IQN	70%	60.73	70%	94.28
Ours (GRU)	86%	61.90	85%	63.86
Ours (GRU)*	84%	63.02	79%	66.19
Ours (MarineFormer)	90%	61.94	86%	61.81
Ours (MarineFormer)*	91%	60.71	81%	64.40

TABLE I: Success rate and path length results.

and we clip the global norm of the gradient at 0.5. The entropy coefficient after 15000 updates increases linearly to encourage exploration. We evaluate our proposed model and the baseline approaches in the two scenarios of Figs. 1c and 1d, described earlier. We test all methods with 500 random unseen test cases. The evaluation metrics include the success rate (SR), and path length (PL) in meters for all the episodes including failed ones. If the USV cannot reach the goal within the episode time limit, or it collides with an obstacle, the test episode is considered failed.

In Tab. I we compare our method to the baseline methods. For methods with an asterisk, we add zero mean Gaussian noise with a standard deviation of 0.1 to the observations of the flow velocity field to examine the robustness of our RL policy to the noisy measurements of the current flow. Tab. I shows that our method achieves the highest success rates across different levels of environment complexity. The results indicate that the Adaptive IQN achieves a maximum SR of 70% while MarineFormer achieves 90% and 86% for scenarios I and II, respectively. The results from Adaptive IQN are comparable with DQN, and they marginally improve the reaction-based APF approach. The results from ORCA show the lowest success rate, as it does not account for the environmental disturbances from the current flow. Almost all the methods in Tab. I show lower SR for scenario II compared to scenario I. The reason is that the environment in the former is more densely populated with obstacles, making navigation more challenging. The MarineFormer achieves the best PL across all methods. The results also show that using transformer leads to better policy compared to using GRU in both scenarios. The superior performance of MarineFormer persists under the noisy measurement case. In addition, as the noise in current flow measurement increases, Ours (MarineFormer)* shows better robustness.

Eight representative navigation routes for various methods are qualitatively compared in Fig. 3. Since dynamic obstacles are constantly changing position, they are not shown in the trajectory images; however, they can be viewed in the supplementary videos and on this article's GitHub page. In Fig. 3a the trajectories of Adaptive IQN and DQN agents are highly affected by flow disturbances due to vortices, trapping them and preventing their successful completion of the episodes. In Fig. 3b, MarineFormer demonstrates better steering control near obstacles compared to other methods. Although the GRU implementation of our method underperforms relative

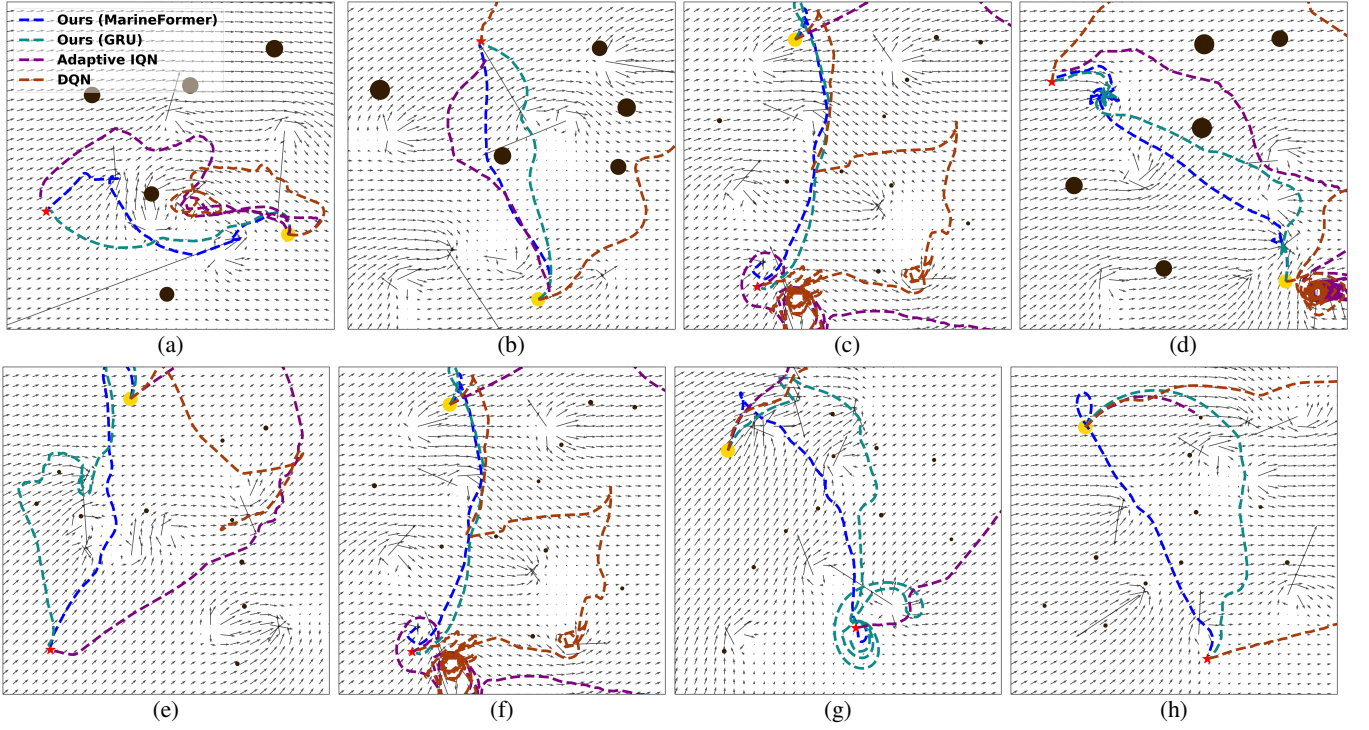


Fig. 3: Representative trajectories of Ours (MarineFormer), Ours (GRU), Adaptive IQN, and DQN for randomly initialized environments. The top and bottom rows, respectively, show the results associated with scenarios I and II.

to MarineFormer, it still significantly outperforms Adaptive IQN and DQN, highlighting the value of our proposed spatial attention. The steering angles for obstacle avoidance in Adaptive IQN and DQN are excessively large, increasing the path length. In Fig. 3c, the trajectory of our proposed method is robust to the strong current flow disturbances near the start point, whereas both Adaptive IQN and DQN experience strong deviations. As the navigation progresses, MarineFormer successfully maneuvers in between two static obstacles. At the same time, the trajectory of the GRU-based method is disrupted by the upstream current source, ultimately leading to a collision. Fig. 3d indicates that, unlike the greedy behavior of baseline methods, our method can effectively find a balance between avoiding collisions and not getting caught in vortices. Fig. 3e shows that almost all the agents successfully reach the target, however, the trajectory of MarineFormer is the least affected by the disturbances from current flow. Fig. 3f exhibits several vortices in the environment. The result shows that both MarineFormer and the GRU implementation of the same architecture, manage to navigate through the vortices while adaptive IQN and DQN struggle to reach the target position. As before, MarineFormer indicates a much more optimal behavior and shorter path length than GRU. Fig. 3g displays another environment with complex hydrodynamics, featuring a sink near the start point and a source close to the goal, along with several other singularities. The results demonstrate that the high-intensity flow at the start point significantly affects the baseline methods. At the target point, the behavior of the

r_t^{do}	r_t^{so}	r_t^f	Alignment score	Current flow observation	SR	PL
✓	✓	✓	✓	✓	90%	63.94
✗	✓	✓	✓	✓	71%	65.33
✓	✗	✓	✓	✓	77%	63.95
✓	✓	✗	✓	✓	65%	67.50
✓	✓	✓	✗	✓	83%	62.82
✓	✓	✓	✓	✗	71%	70.40

TABLE II: Ablation study on the components of the proposed method in scenario I. Included component marked by ✓, and excluded marked by ✗.

GRU-based method is heavily influenced by the source. Fig. 3h shows a vortex close to the goal. MarineFormer navigates around the vortex edge and proceeds with minimal deviation from a straight path. GRU implementation of our method follows a longer path. Adaptive IQN fails to complete the episode and DQN follows an extremely long path, heavily influenced by the flow. The results indicate that the policy learned by our methods and in particular, MarineFormer enables more proactive and long-sighted decision-making and control, especially in challenging marine environments in the presence of large number of dynamic and static obstacles as well as high-flow disturbances.

D. Ablation Study

We conduct an ablation study on the impact of different components of our proposed method. Tab. II shows how

removing individual elements of the architecture affects performance in scenario I. The results indicate that all the reward components r_t^{do} , r_t^{so} and r_t^{cf} have a significant impact on the performance of our method, while the impact of r_t^{cf} on the policy is more prominent. This highlights the importance of guiding the USV's policy not only to avoid obstacles but also to make consistent progress toward the target. We also see that the incorporation of alignment scores leads to at least 7% higher SR. Tab. II shows that removing local measurements of the current flow from the architecture leads to a 19% drop in SR and nearly 7m increase in PL. When the USV is aware of the intensity and direction of the current flow in its surroundings, it can steer toward paths that are minimally impacted by external forces.

V. CONCLUSION

In this work, we introduced MarineFormer, a transformer-based navigation policy featuring spatial attention to environmental factors designed for USVs in complex marine settings including a dense mix of dynamic and static obstacles as well as variable and high-intensity current flows. By leveraging spatial attention to environmental disturbances and obstacles and temporal attention through the transformer to capture the dynamics of interactions, MarineFormer effectively navigates through environments that traditional methods struggle to handle. Our results demonstrate that this approach significantly improves navigation success rates and trajectory efficiency compared to state-of-the-art baselines, particularly in environments with high flow intensity and obstacle density. This study underscores the importance of attention-based architectures for safe, efficient USV navigation. Future work will focus on deploying the developed architecture on real-world USVs.

REFERENCES

- [1] A. Vagale, R. Oucheikh, R. T. Bye, O. L. Osen, and T. I. Fossen, "Path planning and collision avoidance for autonomous surface vehicles i: a review," *Journal of Marine Science and Technology*, pp. 1–15, 2021.
- [2] V. Ashish, "Attention is all you need," *Advances in neural information processing systems*, vol. 30, p. I, 2017.
- [3] M. Hausknecht and P. Stone, "Deep recurrent q-learning for partially observable mdps," in *2015 aaai fall symposium series*, 2015.
- [4] X. Lin, Y. Huang, F. Chen, and B. Englot, "Decentralized multi-robot navigation for autonomous surface vehicles with distributional reinforcement learning," in *2024 IEEE International Conference on Robotics and Automation (ICRA)*. IEEE, 2024.
- [5] Y. Liu, R. Song, R. Bucknall, and X. Zhang, "Intelligent multi-task allocation and planning for multiple unmanned surface vehicles (usvs) using self-organising maps and fast marching method," *Information Sciences*, vol. 496, pp. 180–197, 2019.
- [6] X. Fan, Y. Guo, H. Liu, B. Wei, and W. Lyu, "Improved artificial potential field method applied for auv path planning," *Mathematical Problems in Engineering*, vol. 2020, no. 1, p. 6523158, 2020.
- [7] J. Van Den Berg, S. J. Guy, M. Lin, and D. Manocha, "Reciprocal n-body collision avoidance," in *Robotics Research: The 14th International Symposium ISRR*. Springer, 2011, pp. 3–19.
- [8] S. Liu, P. Chang, Z. Huang, N. Chakraborty, K. Hong, W. Liang, D. L. McPherson, J. Geng, and K. Driggs-Campbell, "Intention aware robot crowd navigation with attention-based interaction graph," in *2023 IEEE International Conference on Robotics and Automation (ICRA)*. IEEE, 2023, pp. 12015–12021.
- [9] V. Zambaldi, D. Raposo, A. Santoro, V. Bapst, Y. Li, I. Babuschkin, K. Tuyls, D. Reichert, T. Lillicrap, E. Lockhart, *et al.*, "Deep reinforcement learning with relational inductive biases," in *International conference on learning representations*, 2019.
- [10] L. C. Melo, "Transformers are meta-reinforcement learners," in *international conference on machine learning*. PMLR, 2022, pp. 15 340–15 359.
- [11] E. Parisotto, F. Song, J. Rae, R. Pascanu, C. Gulcehre, S. Jayakumar, M. Jaderberg, R. L. Kaufman, A. Clark, S. Noury, *et al.*, "Stabilizing transformers for reinforcement learning," in *International conference on machine learning*. PMLR, 2020, pp. 7487–7498.
- [12] A. Banino, A. P. Badia, J. Walker, T. Scholtes, J. Mitrovic, and C. Blundell, "Coberl: Contrastive bert for reinforcement learning," *arXiv preprint arXiv:2107.05431*, 2021.
- [13] Y. Ma, M. Hu, and X. Yan, "Multi-objective path planning for unmanned surface vehicle with currents effects," *ISA transactions*, vol. 75, pp. 137–156, 2018.
- [14] J. Meng, Y. Liu, R. Bucknall, W. Guo, and Z. Ji, "Anisotropic gmp2: A fast continuous-time gaussian processes based motion planner for unmanned surface vehicles in environments with ocean currents," *IEEE Transactions on Automation Science and Engineering*, vol. 19, no. 4, pp. 3914–3931, 2022.
- [15] W. Lan, X. Jin, T. Wang, and H. Zhou, "Improved rrt algorithms to solve path planning of multi-glider in time-varying ocean currents," *IEEE Access*, vol. 9, pp. 158 098–158 115, 2021.
- [16] W. Sun, P. Tsiotras, T. Lolla, D. N. Subramani, and P. F. Lermusiaux, "Multiple-pursuer/one-evader pursuit–evasion game in dynamic flow-fields," *Journal of guidance, control, and dynamics*, vol. 40, no. 7, pp. 1627–1637, 2017.
- [17] M. Xi, J. Yang, J. Wen, H. Liu, Y. Li, and H. H. Song, "Comprehensive ocean information-enabled auv path planning via reinforcement learning," *IEEE Internet of Things Journal*, vol. 9, no. 18, pp. 17 440–17 451, 2022.
- [18] M. Khalid, L. Pénard, and E. Mémin, "Optical flow for image-based river velocity estimation," *Flow Measurement and Instrumentation*, vol. 65, pp. 110–121, 2019.
- [19] X. Lin, J. McConnell, and B. Englot, "Robust unmanned surface vehicle navigation with distributional reinforcement learning," in *2023 IEEE/RSJ International Conference on Intelligent Robots and Systems (IROS)*. IEEE, 2023, pp. 6185–6191.
- [20] D. J. Acheson, *Elementary fluid dynamics*. Oxford University Press, 1990.
- [21] T. Lolla, P. F. Lermusiaux, M. P. Ueckermann, and P. J. Haley, "Time-optimal path planning in dynamic flows using level set equations: theory and schemes," *Ocean Dynamics*, vol. 64, pp. 1373–1397, 2014.
- [22] J. Van den Berg, M. Lin, and D. Manocha, "Reciprocal velocity obstacles for real-time multi-agent navigation," in *2008 IEEE international conference on robotics and automation*. Ieee, 2008, pp. 1928–1935.
- [23] W. Dabney, G. Ostrovski, D. Silver, and R. Munos, "Implicit quantile networks for distributional reinforcement learning," in *International conference on machine learning*. PMLR, 2018, pp. 1096–1105.
- [24] V. Mnih, K. Kavukcuoglu, D. Silver, A. A. Rusu, J. Veness, M. G. Bellemare, A. Graves, M. Riedmiller, A. K. Fidjeland, G. Ostrovski, *et al.*, "Human-level control through deep reinforcement learning," *nature*, vol. 518, no. 7540, pp. 529–533, 2015.
- [25] J. Schulman, F. Wolski, P. Dhariwal, A. Radford, and O. Klimov, "Proximal policy optimization algorithms," *arXiv preprint arXiv:1707.06347*, 2017.